PRAMANA
— journal of
physics

Vol. 79, No. 6
December 2012
pp. 1407–1423

Transverse momentum distributions of identified particles produced in pp, $p(d)A$, and AA collisions at high energies

YA-QIN GAO, CAI-XING TIAN, MAI-YING DUAN, BAO-CHUN LI and FU-HU LIU*

Institute of Theoretical Physics, Shanxi University, Taiyuan, Shanxi 030006, China
*Corresponding author. E-mail: fuhuliu@sxu.edu.cn

MS received 23 February 2012; revised 16 May 2012; accepted 29 May 2012

Abstract. Using a unified description on multiplicity distributions of final-state particles, the transverse momentum distributions of identified particles produced in proton–proton (pp), proton– and deuteron–nucleus [$p(d)A$], and nucleus–nucleus (AA) collisions at high energies are studied in this paper. We assume that the transverse momentum distributions of identified particles measured in final state are contributed by a few energy sources which can be regarded as partons or quarks in the interacting system. The particle is contributed by each source with gluons which have transverse momentum distributions in an exponential form. The modelling results are compared and found to be in agreement with the experimental data at high energies.

Keywords. Unified description; transverse momentum distributions of identified particles; interacting system; pp, $p(d)A$, and AA collisions at high energies.

PACS Nos 25.75.–q; 25.75.Dw

1. Introduction

Transverse momentum (p_{T}) or transverse mass (m_{T}) distributions of identified particles are important experimental measurements in high-energy collisions [1–5]. It is expected that the p_{T} distributions in proton–proton (pp), proton– and deuteron–nucleus [$p(d)A$], and nucleus–nucleus (AA) collisions are different in distribution range and shape owing to different participant numbers and cold nuclear effects [6–10]. For a given $p(d)A$ or AA collisions, the p_{T} distributions are related with impact factor or centrality owing to the same reason. In addition, for a selected event sample, different particles are expected to have different p_{T} distributions.

A few modelling or (semi-)empirical formulas are used in the descriptions of p_{T} (or m_{T}) distributions. For example [11], the p_{T}-exponential: $(\mathrm{d}N/p_{\mathrm{T}}\mathrm{d}p_{\mathrm{T}}) = C_1 \exp(-p_{\mathrm{T}}/T_{p_{\mathrm{T}}})$, the p_{T}^2-exponential or p_{T}-Gaussian: $(\mathrm{d}N/p_{\mathrm{T}}\mathrm{d}p_{\mathrm{T}}) = C_2 \exp(-p^2/T_{p_{\mathrm{T}}}^2)$, the p_{T}^3-exponential: $(\mathrm{d}N/p_{\mathrm{T}}\mathrm{d}p_{\mathrm{T}}) = C_3 \exp(-p^3/T_{p_{\mathrm{T}}}^3)$, the m_{T}-exponential: $(\mathrm{d}N/m_{\mathrm{T}}\mathrm{d}m_{\mathrm{T}}) =$

DOI: 10.1007/s12043-012-0350-1; ***e*Publication: 30 August 2012**

$C_4 \exp(-m_T/T_{m_T})$, the Boltzmann: $(dN/m_T dm_T) = C_5 m_T \exp(-m_T/T_B)$, and the Bose–Einstein distribution: $(dN/m_T dm_T) = C_6[\exp(-m_T/T_{BE}) - 1]^{-1}$, where N denotes the particle number; T_{p_T}, T_{m_T}, T_B, and T_{BE} are fit parameters; and C_1, C_2, C_3, C_4, C_5, and C_6 are normalization constants. These formulas give different shapes in the descriptions of p_T distribution. In low-, intermediate-, and high-p_T ranges, we can use different formulas to fit the experimental data. In a wide p_T range, a two-component formula or a combination of two or three formulas can be used in the investigations.

The STAR Collaboration [11] measured the p_T spectra of $\pi^{\pm}$, $K^{\pm}$, $\bar{p}$, and p in d–Au and Au–Au collisions at the Relativistic Heavy Ion Collider (RHIC) energies and found that the experimental data are well described by the hydrodynamics-motivated blast-wave model [12–18]. The blast-wave model makes the simple assumption that particles are locally thermalized in a hard-sphere uniform density source at a kinetic free-out temperature (T_{kin}) and are moving with a common collective transverse radial flow velocity (β) field. The p_T distribution given by the blast-wave model is [12]

$$\frac{dN}{p_T dp_T} = C_0 \int_0^R r dr m_T I_0\left(\frac{p_T \sinh\rho}{T_{kin}}\right) K_1\left(\frac{m_T \cosh\rho}{T_{kin}}\right),$$

where $\rho = \tanh^{-1}\beta$, I_0 and K_1 are the modified Bessel functions, and C_0 is the normalization constant. In the description of p_T distribution at the RHIC energies, the STAR Collaboration has used a flow velocity profile of the form $\beta = \beta_S(r/R)^n$, where β_S is the surface velocity and r/R is the relative radial position in the thermal source. The exponent of the assumed flow velocity profile, n, is a free parameter [11]. In the blast-wave fit of the STAR Collaboration, the low-p_T part of the pion spectra ($p_T < 0.5$ GeV/c) are excluded due to significant contributions from resonance decays [11].

In our previous work [19,20], a two-component p_T-Gaussian distribution is used to analyse the particle p_T distributions in $\pi^+ p$ interactions at high energy; and a two-component integral p_T-Gaussian distribution is used to describe the particle p_T distributions in pp, $p(d)A$, and AA collisions at high energies. Recently, we proposed a unified description on multiplicity distributions of final-state products in different collision systems at high energies [21] and studied isotopic production cross-sections of nuclear fragments in pA and AA reactions at intermediate and high energies [22] using the unified formula. Although the particle p_T distributions are different from the particle multiplicity distributions and the fragment isotopic cross-sections, it is expected that our model can be directly used to describe the p_T spectra of final-state identified particles produced in pp, $p(d)A$, and AA collisions at high energies. In this paper, we shall use the unified formula [20] to describe the particle p_T distributions and compare our calculated results with the available experimental data.

2. The model

In our recent work [21], a unified formula was proposed to describe the multiplicity distributions of the final-state products produced in e^+e^-, pp, $p\bar{p}$, e^+p, pA, and AA collisions at high energies. If we regard the neutron number in a nuclide as the neutron multiplicity in a final state, the unified formula can be used to analyse the isotopic production cross-sections of nuclear fragments [22]. The main idea of our model is that many emission

sources of particles and fragments are assumed to form in collisions. The multiplicity distribution is contributed by each source in an exponential form. If we regard a given particle p_{T} as a result of multisource contributions, the unified formula can be used to describe the p_{T} spectra of identified particles. Although the model used in the present work can be found in our recent work [20,21], we explain the model in the following section in terms of p_{T} and its distribution for the whole presentation of the present work.

In the model, we assume that each final-state particle is formed by the contributions of a few internal energy sources. These energy sources could be quark-gluon plasma, unconfined QCD plasma, partons, or the more model-independent prematter. We would like to use partons or quarks as the energy sources in the present work. The energy sources of a considered particle are divided into l groups due to different contribution mechanisms. The energy source number in the jth group is assumed to be m_j. Each energy source contributes internal energy distribution in an exponential form. The contributed momentum of the source has an exponential distribution when the rest mass of the transporter is neglected. For a particle with a given emission angle, its transverse momentum is proportional to the obtained momentum. Then, the transverse momentum (p_{tij}) distribution contributed by the ith source in the jth group is assumed to obey

$$P_{ij}(p_{tij}) = \frac{1}{\langle p_{tij}\rangle}\exp\left(-\frac{p_{tij}}{\langle p_{tij}\rangle}\right), \tag{1}$$

where $\langle p_{tij}\rangle = \int p_{tij}P_{ij}(p_{tij})\mathrm{d}p_{tij}$ is the mean transverse momentum contributed by the ith source in the jth group. Generally, we assume $\langle p_{t1j}\rangle = \langle p_{t2j}\rangle = \cdots = \langle p_{tm_jj}\rangle = T$, where T is the fit parameter. The particle p_{T} distribution contributed by the jth group is then given by the folding of m_j exponential functions. That is, we have an Erlang distribution

$$P_j(p_{\mathrm{T}}) = \frac{p_{\mathrm{T}}^{m_j-1}}{(m_j-1)!\langle p_{tij}\rangle^{m_j}}\exp\left(-\frac{p_{\mathrm{T}}}{\langle p_{tij}\rangle}\right). \tag{2}$$

The p_{T} distribution contributed by l groups is given by a weighted sum of l Erlang distributions

$$P(p_{\mathrm{T}}) = \frac{1}{N}\frac{\mathrm{d}N}{\mathrm{d}p_{\mathrm{T}}} = \sum_{j=1}^{l} k_j P_j(p_{\mathrm{T}}), \tag{3}$$

where k_j denotes the weight factor. Generally, $k_1 + k_2 + \cdots + k_l = 1$.

In the above discussions, m_j denotes the source number in the jth group. To avoid calculation of $(m_j - 1)!$ when $m_j - 1$ is too large, we use the Monte Carlo method to calculate the p_{T} distribution. Let R_{ij} denote random variable in [0,1]. The exponential distribution given by eq. (1) results in

$$p_{tij} = -\langle p_{tij}\rangle \ln R_{ij}. \tag{4}$$

The particle p_{T} contributed by the jth group can be obtained by

$$p_{\mathrm{T}} = -\sum_{i=1}^{m_j}\langle p_{tij}\rangle \ln R_{ij} \tag{5}$$

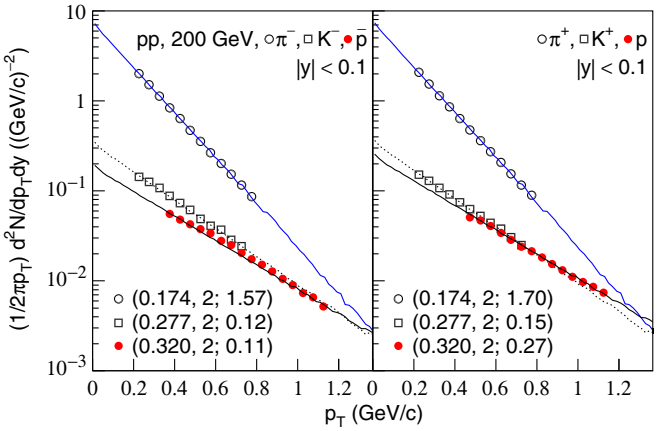

Figure 1. The p_{T} spectra of $\pi^{\pm}$, $K^{\pm}$, $\bar{p}$, and p produced in pp collisions at $\sqrt{s} =$ 200 GeV. The symbols represent the experimental data of the STAR Collaboration [11] and the curves are our calculated results by two sources with two parameters.

owing to it being the folding of m_j exponential functions. The p_{T} distribution contributed by the l groups is finally obtained by a statistical method after considering the weight factor k_j. The mean p_{T} is then given by

$$\langle p_{\mathrm{T}} \rangle = \sum_{j=1}^{l} k_j \langle p_{tij} \rangle m_j. \tag{6}$$

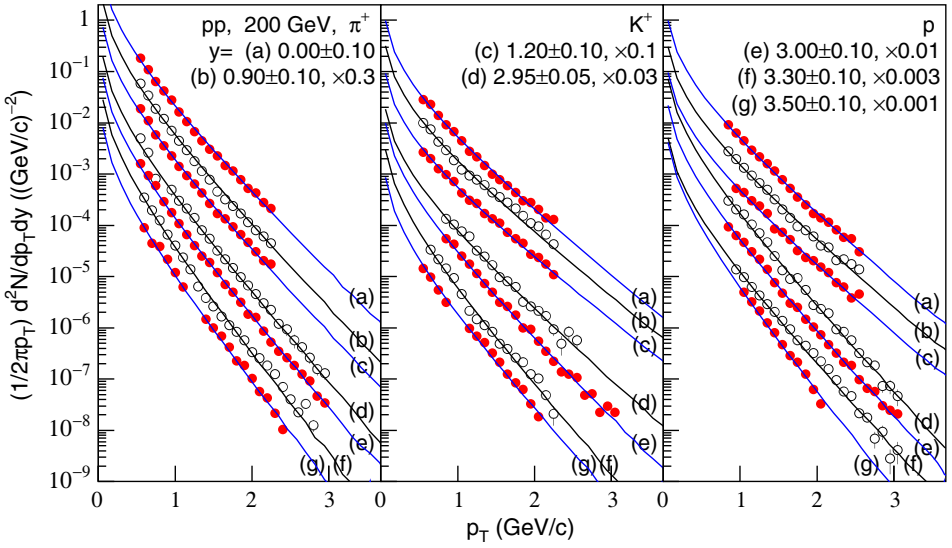

Figure 2. The p_{T} spectra of π^{+}, K^{+}, and p produced in pp collisions at $\sqrt{s} =$ 200 GeV for seven rapidity bins. The symbols represent the experimental data of the BRAHMS Collaboration [28] and the curves are our calculated results by one source with two parameters.

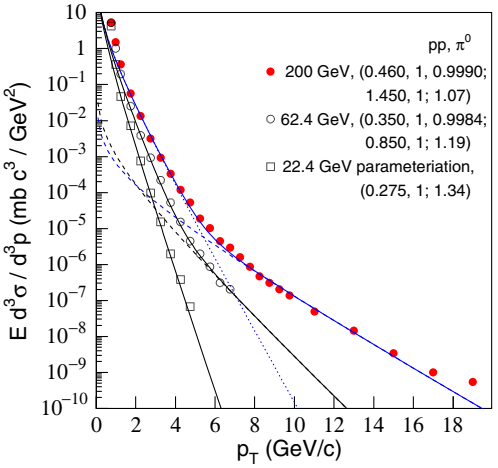

Figure 3. Invariant π^0 cross-sections in pp collisions at $\sqrt{s} = 200$, 62.4, and 22.4 GeV. The symbols represent the experimental data or parameteriation of the PHENIX Collaboration [29]. The curves are our calculated results, where the dotted and dashed curves are the contributions of the first and second source groups respectively. Both the solid curves for $\sqrt{s} = 200$ and 62.4 GeV are obtained by 1+1 sources with five parameters. The curve for $\sqrt{s} = 22.4$ GeV is obtained by one source with two parameters.

The number of free parameters in the present model is $3l - 1$. When $l = 1$, the free parameters are $\langle p_{ti1}\rangle$ and m_1. When $l = 2$, the free parameters are $\langle p_{ti1}\rangle$, m_1, k_1, $\langle p_{ti2}\rangle$, and m_2. Generally, $l = 1$ or $l = 2$ can describe the p_{T} distributions. In addition,

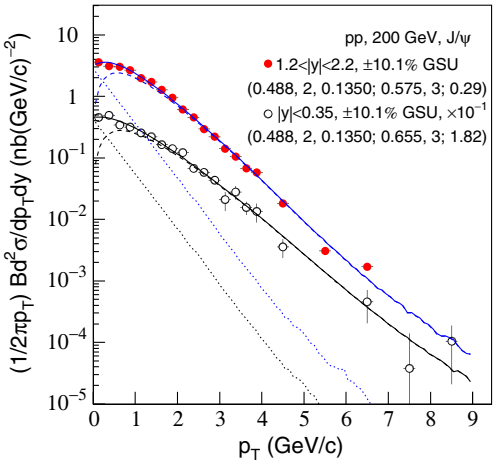

Figure 4. J/ψ differential cross-section times dilepton branching ratio vs. p_{T} in pp collisions at $\sqrt{s} = 200$ GeV. The symbols represent the experimental data of the PHENIX Collaboration [30,31]. Both the solid curves are our calculated results by 2+3 sources with five parameters. The dotted and dashed curves are the contributions of the first and second source groups respectively.

Table 1. Values of parameters and χ^2/DOF for the fits in figure 2. The unit of $\langle p_{tij} \rangle$ is GeV/c.

Rapidity	Particle	$\langle p_{ti1} \rangle$	m_1	χ^2/DOF	Rapidity	Particle	$\langle p_{ti1} \rangle$	m_1	χ^2/DOF
0.00 ± 0.10	π^+	0.315	1	0.32	3.00 ± 0.10	π^+	0.270	1	0.83
	K^+	0.391	1	1.03		K^+	0.316	1	0.86
	p	0.378	1	0.99		p	0.293	1	0.82
0.90 ± 0.10	π^+	0.300	1	0.41	3.30 ± 0.10	π^+	0.246	1	1.23
	K^+	0.400	1	1.02		K^+	0.276	1	1.20
	p	0.378	1	1.00		p	0.293	1	0.87
1.20 ± 0.10	π^+	0.300	1	0.30	3.50 ± 0.10	π^+	0.245	1	1.22
	K^+	0.410	1	0.97		K^+	0.283	1	1.44
	p	0.378	1	1.05		p	0.253	1	1.89
2.95 ± 0.05	π^+	0.275	1	0.79					
	K^+	0.356	1	1.04					
	p	0.290	1	0.87					

the present model does not answer what the sources are. In the framework of a combination model of constituent quarks and Landau hydrodynamics [23,24], we may regard the sources as quarks and gluons. In the framework of a two-stage gluon model or a gluon dominance model [25–27], the sources can be regarded as active gluons and evaporated gluons. Generally, the sources can be partons because the sources of the considered

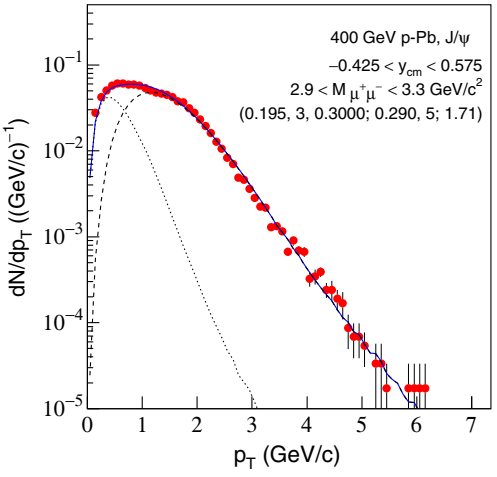

Figure 5. The p_{T} distribution, $\mathrm{d}N/\mathrm{d}p_{\mathrm{T}}$, of J/ψ particles produced in p–Pb collisions at an incident energy of 400 GeV. The symbols represent the experimental data of the NA50 Collaboration [32]. The solid curve is our calculated result by 3+5 sources with five parameters. The dotted and dashed curves are the contributions of the first and second source groups respectively.

particles in pp, $p(d)A$, and AA collisions are the same partons. We can give a unified description for different collisions.

3. Comparisons with experimental data

The p_T spectra, in different presentation forms as used in [11,28–31], for identified particles emitted in pp collisions at different centre-of-mass energies are shown in figures 1–4, where y, E, p, σ, and B denote the rapidity, energy, momentum, cross-section, and dilepton branching ratio respectively. The symbols at the centre-of-mass energy $\sqrt{s} = 200$ and 62.4 GeV represent the experimental data of the STAR, BRAHMS, and PHENIX Collaborations [11,28–31]; and the symbols at 22.4 GeV are the parameteriation of the PHENIX Collaboration [29]. Some experimental data are selected in different rapidity bins (figure 2) and with different global scale uncertainties (GSUs) (figure 4), with each scaled by the amount indicated in the legend. The curves are our calculated results by fitting the experimental data or parameteriation with $j = 1$ (figures 1, 2 and 3 (at 22.4 GeV)) or $j = 2$ (figures 3 (at 200 and 62.4 GeV) and 4). The dotted and dashed curves

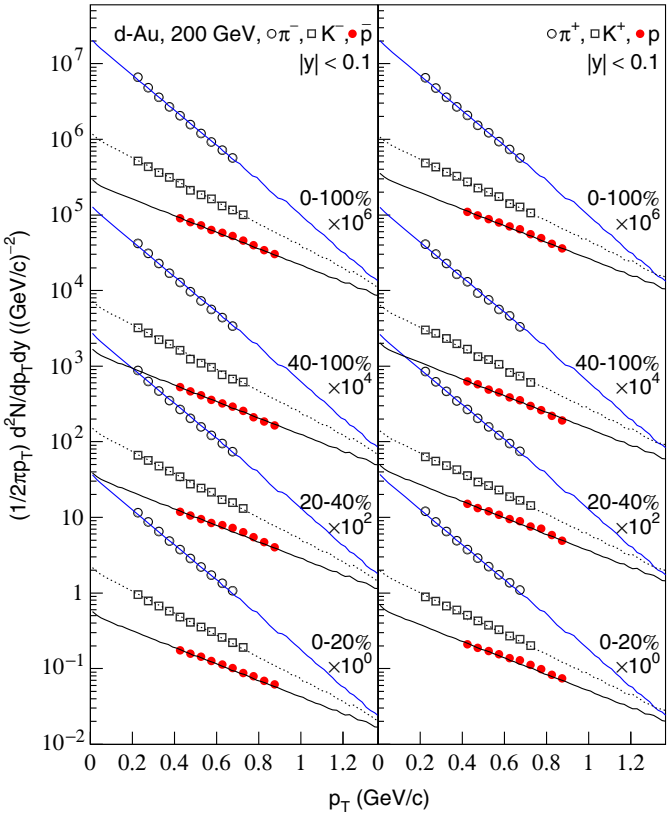

Figure 6. As for figure 1, but showing the results of d–Au collisions at $\sqrt{s_{NN}} =$ 200 GeV for minimum bias sample and three centrality classes.

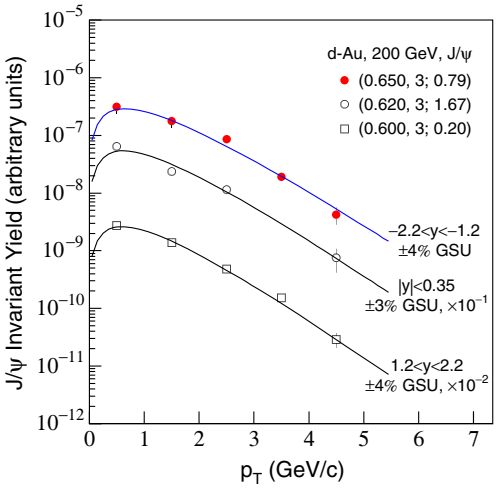

Figure 7. J/ψ invariant yield vs. p_{T} in d–Au collisions at $\sqrt{s_{NN}} = 200$ GeV. The symbols represent the experimental data of the PHENIX Collaboration [33] and the curves are our calculated results by three sources with two parameters.

when $j = 2$ denote the contributions of the first and second source groups respectively. The values of fit parameters and χ^2 per degree of freedom (χ^2/DOF) for the fits in figure 2 are given in table 1, and for the fits in figures 1, 3, and 4 are given in the figures in terms of '($\langle p_{ti1}\rangle$, m_1; χ^2/DOF)' when $j = 1$ or '($\langle p_{ti1}\rangle$, m_1, k_1; $\langle p_{ti2}\rangle$, m_2; χ^2/DOF)' when $j = 2$. The unit of $\langle p_{tij}\rangle$ is GeV/c. One can see that the model describes the experimental data of pp collisions at the RHIC energies.

The p_{T} distribution, $\mathrm{d}N/\mathrm{d}p_{\mathrm{T}}$, of J/ψ particles produced in p–Pb collisions at incident beam energy $E_{\mathrm{beam}} = 400$ GeV (the superproton synchrotron (SPS) energy) is presented

Table 2. Values of parameters and χ^2/DOF for the fits in figure 6. The unit of $\langle p_{tij}\rangle$ is GeV/c.

Centrality	Particle	$\langle p_{ti1}\rangle$	m_1	χ^2/DOF	Particle	$\langle p_{ti1}\rangle$	m_1	χ^2/DOF
0–100%	π^-	0.187	2	1.10	π^+	0.187	2	1.05
	K^-	0.299	2	0.25	K^+	0.322	2	0.16
	$\bar{p}$	0.398	2	0.09	p	0.398	2	0.10
40–100%	π^-	0.187	2	1.29	π^+	0.187	2	1.31
	K^-	0.299	2	0.30	K^+	0.322	2	0.09
	$\bar{p}$	0.398	2	0.19	p	0.398	2	0.19
20–40%	π^-	0.187	2	1.44	π^+	0.187	2	1.06
	K^-	0.299	2	0.19	K^+	0.322	2	0.15
	$\bar{p}$	0.398	2	0.13	p	0.398	2	0.12
0–20%	π^-	0.187	2	0.77	π^+	0.187	2	0.95
	K^-	0.299	2	0.23	K^+	0.322	2	0.17
	$\bar{p}$	0.398	2	0.06	p	0.398	2	0.13

in figure 5. The circles are the experimental data, in a given centre-of-mass rapidity $y_{\rm cm}$ and invariant mass $M_{\mu^+\mu^-}$-ranges, of the NA50 Collaboration [32]. The solid curve is our calculated results with $j = 2$, the dotted and dashed curves are the contributions of the first and second source groups respectively, and the corresponding parameter values are given in the figure. Once more the model describes the experimental data of pA collisions at the SPS energy.

Figures 6 and 7 display the $p_{\rm T}$ spectra of identified particles produced in d–Au collisions at the RHIC energy. The STAR [11] and PHENIX [33] experimental data are selected in different centralities (figure 6) and different rapidities with different GSUs (figure 7) respectively. The curves are our calculated results and the parameter values are given in table 2 (for the fits in figure 6) and figure 7 (for the fits in figure 7). One can see a successful modelling description of the considered experimental data. We would like to point out that there are differences in $\langle p_{\rm T}\rangle$ as shown in ref. [11] and the parameter $\langle p_{ti1}\rangle$ shown in table 2. This difference is because of two sources being used in the present work, each contributing $\langle p_{ti1}\rangle = \langle p_{\rm T}\rangle/2$, which is half of what is obtained in ref. [11].

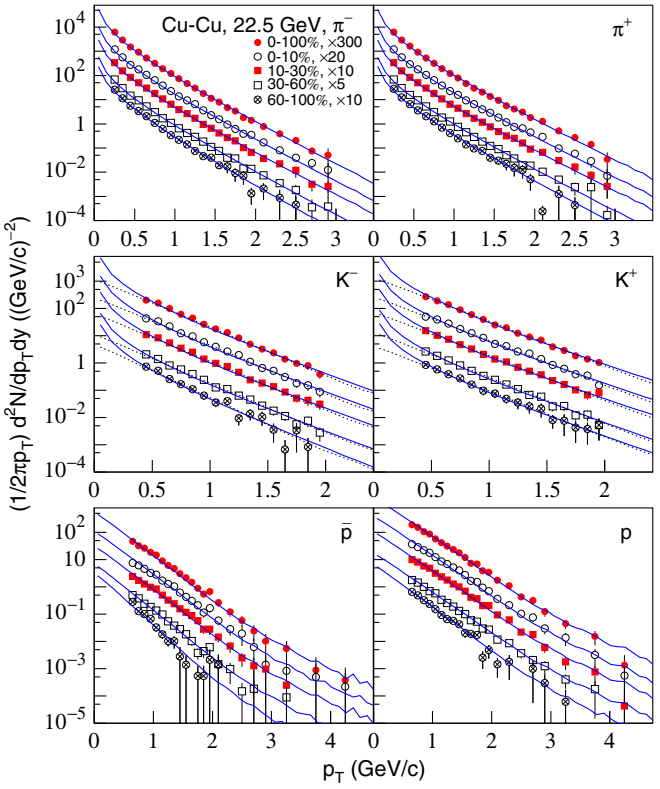

Figure 8. The $p_{\rm T}$ spectra of $\pi^{\pm}$, $K^{\pm}$, $\bar{p}$, and p produced in Cu–Cu collisions at $\sqrt{s_{NN}} = 22.5$ GeV. The symbols represent the experimental data of the PHENIX Collaboration [34] for minimum bias sample and four centrality classes. The solid curves are our calculated results by one source with two parameters, and the dotted curves are given by two sources with two parameters.

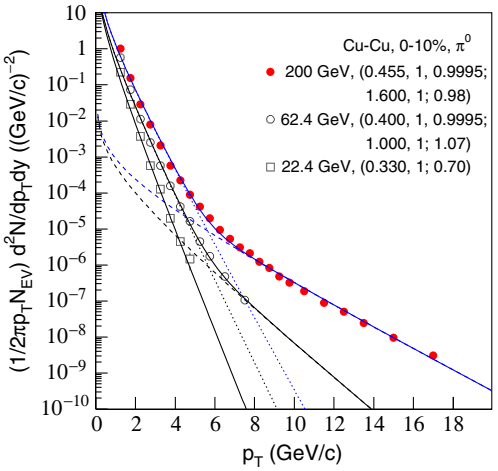

Figure 9. Invariant π^0 yields in Cu–Cu collisions at $\sqrt{s_{NN}} = 200$, 62.4, and 22.4 GeV. The symbols represent the experimental data of the PHENIX Collaboration [29]. The curves are our calculated results, where the dotted and dashed curves are the contributions of the first and second source groups respectively. Both the solid curves for $\sqrt{s_{NN}} = 200$ and 62.4 GeV are obtained by 1+1 sources with five parameters. The curve for $\sqrt{s_{NN}} = 22.4$ GeV is obtained by one source with two parameters.

The p_T spectra of identified particles produced in Cu–Cu collisions at the RHIC energies are given in figures 8 and 9, where N_{EV} in figure 9 denotes the event number. The symbols represent the experimental data of the PHENIX Collaboration [29,34] for

Table 3. Values of parameters and χ^2/DOF for the fits in figure 8. The values under '/' are for the dotted curves. The unit of $\langle p_{tij} \rangle$ is GeV/c.

Centrality	Particle	$\langle p_{ti1} \rangle$	m_1	χ^2/DOF	Particle	$\langle p_{ti1} \rangle$	m_1	χ^2/DOF
0–100%	π^-	0.278	1	0.46	π^+	0.288	1	0.44
	K^-	0.320/0.245	1/2	0.54/0.71	K^+	0.353/0.268	1/2	0.66/0.79
	$\bar{p}$	0.265	2	0.57	p	0.295	2	0.63
60–100%	π^-	0.256	1	0.48	π^+	0.270	1	0.35
	K^-	0.290/0.220	1/2	0.91/0.88	K^+	0.335/0.259	1/2	1.36/0.98
	$\bar{p}$	0.222	2	1.23	p	0.273	2	1.37
30–60%	π^-	0.270	1	0.42	π^+	0.280	1	1.09
	K^-	0.310/0.240	1/2	0.72/0.94	K^+	0.335/0.259	1/2	0.68/0.97
	$\bar{p}$	0.250	2	0.91	p	0.295	2	0.46
10–30%	π^-	0.278	1	0.45	π^+	0.288	1	0.35
	K^-	0.320/0.245	1/2	0.52/0.61	K^+	0.353/0.268	1/2	0.72/0.74
	$\bar{p}$	0.265	2	0.54	p	0.295	2	0.48
0–10%	π^-	0.278	1	0.55	π^+	0.288	1	0.42
	K^-	0.320/0.245	1/2	0.59/0.72	K^+	0.353/0.268	1/2	0.62/0.66
	$\bar{p}$	0.270	2	0.81	p	0.295	2	0.43

different centralities and the curves are our calculated results with $j = 1$ (figures 8 and 9 (at 22.4 GeV)) or $j = 2$ (figure 9 (at 200 and 62.4 GeV)). For comparison, the solid and dotted curves for $K^{\pm}$ spectra in figure 8 are shown by two sets of parameter values. The dotted and dashed curves in figure 9 are the contributions of the first and second source groups respectively. The parameter values are given in table 3 (for the fits in figure 8) and figure 9 (for the fits in figure 9). Once more the model is successful in describing the concerned experimental data. Similar to table 2, for $K^{\pm}$ in table 3, one would expect the same factor of half when two sources are used as compared to when one source is used. However, the situation is not true due to the narrow data range in figure 8. Especially, in the range of $p_{\mathrm{T}} < 0.5$ GeV/c, the differences between the two curves are large. If we consider the data distribution in the low p_{T} range, at least one curve is not acceptable. Theoretically, when the two curves are acceptable, one would expect a factor of $1/2$ when two sources are used compared to when one source is used.

Figures 10 and 11 present the p_{T} spectra of identified particles produced in Au–Au collisions at the RHIC energies. The symbols represent the experimental data of the STAR [10] and PHENIX [35] Collaborations for different centralities and the curves are

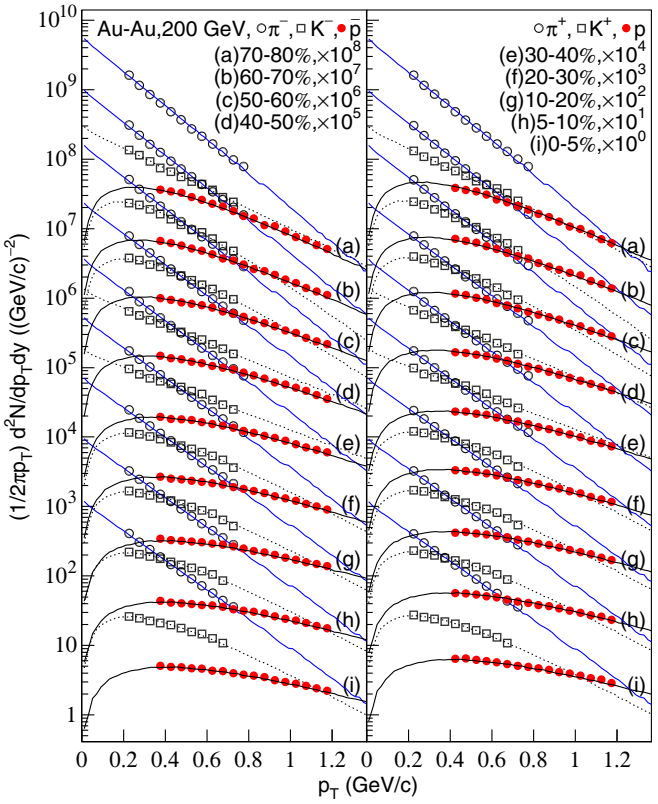

Figure 10. As for figure 1, but showing the results of Au–Au collisions at $\sqrt{s_{NN}} =$ 200 GeV for nine centrality classes. The source numbers are two or three, and the parameter numbers are two.

our calculated results with $j = 1$ (figure 10) and $j = 2$ (figure 11). The dotted and dashed curves in figure 11 are the contributions of the first and second source groups respectively. Corresponding to figures 10 and 11, the parameter values are given in tables 4 and 5 respectively. We would like to point out that in some cases the values of χ^2/DOF for the fits are much below 1. The probable reason is that the point-to-point errors in the data have been overestimated. In fact, in our fits, only two parameters, $\langle p_{ti1} \rangle$ and m_1, have been used in these cases. From the comparisons one can see that the model describes the experimental data of AA collisions at the RHIC energies.

The results in table 4 show that for K^- the fit requires two sources in the centrality class 70–80% whereas it requires three sources in the neighbouring centrality class 60–70%. The data for 40–50% class again fits with two sources. The change in the value of m_1 for different centrality classes for the same particle is caused by the narrow data range. It is assumed that at least one case (two or three sources) is not acceptable in the low p_T range. For the narrow data range, the modelling source number has a fluctuation. To determine the exact source number, a wider data range covering all p_T region is needed.

We notice that the data presented in figures 4 and 7 are shown with different GSUs. This is given by the quoted experimental data [30,31,33]. In other figures, the data do not show the effects of GSUs. We would like to say that the only difference when the GSUs are present or not, is the selected criterion of the quoted data. The fitting processes for the two cases are in fact the same in the present work. In some figures (e.g. figures 4 and 8) a few small kinks appear in the fitted curves at large p_T, because we have used the Monte Carlo method in fitting the experimental data. This fluctuation has no dynamical reason, but only a statistical reason.

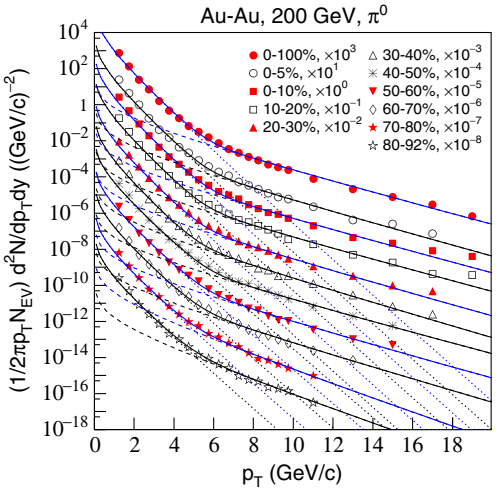

Figure 11. As for figure 10, but showing the results of Au–Au collisions at $\sqrt{s_{NN}} =$ 200 GeV for minimum bias sample and ten centrality classes. The symbols represent the experimental data of the PHENIX Collaboration [35]. The solid curves are our calculated results by 1+1 sources with five parameters, and the dotted and dashed curves correspond to the contributions of the first and second source groups respectively.

Table 4. Values of parameters and χ^2/DOF for the fits in figure 10. The unit of $\langle p_{tij} \rangle$ is GeV/c.

Centrality	Particle	$\langle p_{ti1} \rangle$	m_1	χ^2/DOF	Particle	$\langle p_{ti1} \rangle$	m_1	χ^2/DOF
70–80%	π^-	0.178	2	1.75	π^+	0.178	2	1.43
	K^-	0.300	2	0.19	K^+	0.300	2	0.10
	$\bar{p}$	0.252	3	0.04	p	0.260	3	0.14
60–70%	π^-	0.184	2	1.81	π^+	0.184	2	1.44
	K^-	0.180	3	0.24	K^+	0.180	3	0.24
	$\bar{p}$	0.269	3	0.05	p	0.283	3	0.05
50–60%	π^-	0.189	2	1.40	π^+	0.189	2	1.32
	K^-	0.200	3	0.14	K^+	0.200	3	0.17
	$\bar{p}$	0.293	3	0.05	p	0.306	3	0.07
40–50%	π^-	0.196	2	0.81	π^+	0.196	2	0.82
	K^-	0.350	2	0.14	K^+	0.350	2	0.15
	$\bar{p}$	0.311	3	0.03	p	0.325	3	0.06
30–40%	π^-	0.196	2	1.20	π^+	0.196	2	1.22
	K^-	0.385	2	0.13	K^+	0.385	2	0.13
	$\bar{p}$	0.340	3	0.02	p	0.345	3	0.02
20–30%	π^-	0.200	2	0.96	π^+	0.200	2	1.02
	K^-	0.225	3	0.10	K^+	0.225	3	0.11
	$\bar{p}$	0.356	3	0.07	p	0.355	3	0.03
10–20%	π^-	0.205	2	0.67	π^+	0.205	2	0.60
	K^-	0.225	3	0.13	K^+	0.225	3	0.10
	$\bar{p}$	0.391	3	0.06	p	0.379	3	0.01
5–10%	π^-	0.205	2	1.03	π^+	0.205	2	1.07
	K^-	0.225	3	0.11	K^+	0.225	3	0.14
	$\bar{p}$	0.391	3	0.03	p	0.391	3	0.07
0–5%	π^-	0.205	2	0.94	π^+	0.205	2	0.87
	K^-	0.225	3	0.10	K^+	0.225	3	0.08
	$\bar{p}$	0.407	3	0.02	p	0.407	3	0.03

Table 5. Values of parameters and χ^2/DOF for the fits in figure 11. The unit of $\langle p_{tij} \rangle$ is GeV/c.

Centrality	$\langle p_{ti1} \rangle$	m_1	k_1	$\langle p_{ti2} \rangle$	m_2	χ^2/DOF
0–100%	0.455	1	0.9995	1.600	1	1.13
80–92%	0.475	1	0.9960	1.200	1	0.94
70–80%	0.475	1	0.9960	1.200	1	0.43
60–70%	0.475	1	0.9986	1.450	1	0.71
50–60%	0.482	1	0.9990	1.530	1	1.18
40–50%	0.475	1	0.9993	1.600	1	0.53
30–40%	0.450	1	0.9990	1.450	1	0.59
20–30%	0.455	1	0.9993	1.520	1	0.56
10–20%	0.455	1	0.9995	1.600	1	0.99
0–10%	0.455	1	0.9996	1.600	1	1.11
0–5%	0.455	1	0.9995	1.546	1	1.04

4. Conclusions and discussions

To conclude, the transverse momentum distributions of identified particles produced in pp, $p(d)A$, and AA collisions are studied using a unified formula. This formula was first proposed by us to describe the multiplicity distributions of final-state products produced in 'elementary' particle interactions and heavy-ion collisions at high energies and used to describe the isotopic production cross-sections of nuclear fragments emitted in pA and AA collisions at intermediate energy and the low end of high energies. The basis of the formula is a multisource model in which the contribution of each source is an exponential factor of the considered distribution.

According to the values of $\langle p_{tij}\rangle$, m_j, and k_j given in the figures and tables, the values of mean transverse momentum $\langle p_{\rm T}\rangle$ for different collisions can be obtained by eq. (6). We would like to point out that the modelling values of $\langle p_{\rm T}\rangle$ obtained by eq. (6) are for the whole $p_{\rm T}$ range which are wider than the range of the considered experimental data. The lower and upper cut-offs of $p_{\rm T}$ for the modelling $\langle p_{\rm T}\rangle$ are 0 and ∞ respectively, whereas the lower and upper cut-offs for the experimental one are the minimum and maximum $p_{\rm T}$ in the available data range.

Table 6. Summary of some dependences of $\langle p_{\rm T}\rangle$. The unit of $\langle p_{\rm T}\rangle$ is GeV/c.

Figure	Selection 1	Selection 2	$\langle p_{\rm T}\rangle$	m_1	m_2
Figure 2	π^+	$y = 3.50 \pm 0.10$	0.245	1	–
		$y = 3.30 \pm 0.10$	0.246	1	–
		$y = 3.00 \pm 0.10$	0.270	1	–
		$y = 2.95 \pm 0.05$	0.275	1	–
		$y = 1.20 \pm 0.10$	0.300	1	–
		$y = 0.90 \pm 0.10$	0.300	1	–
		$y = 0.00 \pm 0.10$	0.315	1	–
Figure 9	π^0	$\sqrt{s} = 22.4$ GeV	0.330	1	–
		$\sqrt{s} = 62.4$ GeV	0.400	1	1
		$\sqrt{s} = 200$ GeV	0.456	1	1
Figure 6	0–20%	π^+	0.374	2	–
		K^+	0.644	2	–
		p	0.796	2	–
Figure 6	π^+	40–100%	0.374	2	–
		20–40%	0.374	2	–
		0–20%	0.374	2	–
Figure 10	π^+	70–80%	0.356	2	–
		60–70%	0.368	2	–
		50–60%	0.378	2	–
		40–50%	0.392	2	–
		30–40%	0.392	2	–
		20–30%	0.400	2	–
		10–20%	0.410	2	–
		5–10%	0.410	2	–
		0–5%	0.410	2	–

In comparisons with the data, separate fits are made at each rapidity and centrality. Then the rapidity and centrality dependences of $\langle p_T \rangle$ are empirically obtained. In table 6, some dependences of $\langle p_T \rangle$ are summarized. It is shown that the concerned $\langle p_T \rangle$ increases with decreasing rapidity, increases with increasing centre-of-mass energy and particle mass, and does not depend on centrality or increases slightly with increasing centrality. The number of sources, or the number of effective participant partons, does not show an obvious dependence on rapidity, particle mass, and centrality. This renders that the number of effective partons for producing a particle at a given energy is not related to other conditions, but partons in both the interacting nucleons. For a heavy particle in central rapidity region in higher energy collisions, a higher $\langle p_T \rangle$ is expected to be observed due to stronger parton interactions.

The model uniformly treats the final-state particles and nuclear fragments by the same formula. It is shown that the model is successful in describing multiplicity distributions of final-state particles, isotopic production cross-sections of nuclear fragments, and transverse momentum spectra of identified particles. Of course, as a multicomponent Erlang distribution, eq. (3) has different mean contributions from the ith source in the jth group when different distributions are considered. In the investigations of multiplicity distributions, isotopic cross-sections, and transverse momentum spectra, the mean contributions are the mean multiplicity, mean neutron number, and mean transverse momentum, respectively.

When p_T spectra are considered, the sources may be partons or quarks. In low-, intermediate-, and high-p_T ranges, or for narrow and wide p_T distributions, the modelling results in the present work do not give a large m_j. In fact, in most of the cases we have used $m_j = 1$, 2, or 3; and $j = 1$ to l ($l = 1$ or 2). The number of free parameters in the model is $3l - 1$. For a narrow p_T spectrum which contains the low- and intermediate-p_T parts, we use mostly $l = 1$ in the investigation. For a wide p_T spectrum which contains low-, intermediate-, and high-p_T parts, we have to use $l = 2$ owing to the contributions of two mechanisms or two processes. The present work shows that the number of sources in most cases is in the range of 1–3. This renders that only few partons contribute to the transverse momentum. To give a further test of the parton source assumption, the energy spectra of particles and nuclear fragments, and multiplicity distributions of nuclear fragments should be analysed in the future. On the other hand, this model provides a convenient way to parametrize the data. In most of the cases the number of sources is simply taken to be 1, 2, or 3. The values of $\langle p_{ij} \rangle$ is easily obtained by fitting the data.

It seems that the present work is similar to ref. [21]. However, the physics pictures in the two cases are different. For multiplicity distribution, the data sample is the reaction events, and the sources contribute to the events with multiplicities of particles. For transverse momentum spectrum, the data sample is the produced particles, and the sources contribute to the particles with transverse momenta of gluons. The transverse momentum of the particle which contains a few gluons is the sum of gluon transverse momenta. The energies of the gluons are then transformed to the particle energy. We have investigated the centrality (and rapidity) dependence of p_T distributions in AA (and pp) collisions in the present work. Similarly, the multiplicity dependence of p_T distributions in pp collisions can be described by the model, and $\langle p_T \rangle$ increases slightly with increasing multiplicity.

As we know, the previously fit-models listed in ref. [11] for p_T (or m_T) spectra are successful in a partly p_T range. To give a description in whole p_T range, a two- or three-component distribution is needed. Meanwhile, the distribution shape given by a previously used fit-model [11] is single. From exponential form to Gaussian distribution, the current approach with respect to the previous fits is very flexible, which is also the advantage of the present work. A two- or multi-component Erlang distribution can be used to fit a large amount of data even for the quasipower-law dependence in pp collisions at $\sqrt{s} = 200$ GeV [36] and 7000 GeV [37] and for p_T up to 200 GeV/c at the Large Hadron Collider (LHC) energy [37]. Meanwhile, the current approach is successful in describing multiplicity distributions of final-state particles and nuclear fragments produced in different collision systems at high energies [21] and isotopic production cross-sections of nuclear fragments in pA and AA reactions at intermediate and high energies [22].

We would like to point out that the model presented here manages to fit the data essentially using a sum of distributions from exponential form to Gaussian. In figures 3, 9, and 11, the presence of a transition in the behaviour of the p_T spectrum is evident. In these cases we have used $m_1 = 1$ and $m_2 = 1$ to describe the data. It means that the different behaviours at high p_T comes from an exponential distribution instead of a Gaussian. Of course, with a sufficiently high number of Gaussians it is probably possible to describe any kind of data. But this does not necessarily guarantee that the physics is described in the correct or best way. However, the present work does not give a simple multi-Gaussian, but a unified description in the framework of the multisource model.

The main idea of this model is the superposition of Erlang distributions. Generally, when $m_j > 1$, Erlang distribution reproduces p_T distributions with peaks lower than the maximum of $(p_T/\langle p_{tij}\rangle^2)\exp(-p_T/\langle p_{tij}\rangle)\mathrm{d}p_T$ which is the result of $m_j = 2$. When $m_j = 1$, one can obtain the superposition of exponential distributions which may be more fruitful [38]. We see that the superposition of exponential distributions is a special case of the superposition of Erlang distributions. The latter one is more flexible compared to experimental data.

Acknowledgements

This work was supported by the National Natural Science Foundation of China, Grant No. 10975095, the National Fundamental Fund of Personnel Training, Grant No. J1103210, the Open Research Subject of the Chinese Academy of Sciences Large-Scale Scientific Facility Grant, No. 2060205, and the Shanxi Scholarship Council of China.

References

[1] STAR Collaboration: O Barannikova, *Nucl. Phys.* **A774**, 465 (2006)
[2] T Renk and J Ruppert, *Phys. Rev.* **C77**, 024907 (2008)
[3] S Mrowczynski, *Phys. Rev.* **C73**, 044907 (2006)
[4] CERES Collaboration: M Płoskoń, *Nucl. Phys.* **A783**, 527c (2007)
[5] G Fai, P Lévai and G Papp, *Nucl. Phys.* **A783**, 535c (2007)
[6] K Grebieszkow, *Phys. Rev.* **C76**, 064908 (2007)
[7] M B Johnson, B Z Kopeliovich, M J Leitch, P L McGaughey, J M Moss, I K Potashnikova and I Schmidt, *Phys. Rev.* **C75**, 035206 (2007)

[8] E G Ferreiro, F Fleuret, J P Lansberg and A Rakotozafindrabe, *Phys. Lett.* **B680**, 50 (2009)
[9] C Loizides, *Eur. Phys. J.* **C49**, 339 (2007)
[10] A M Rakotozafindrabe, *AIP Conf. Proc.* **1038**, 63 (2008)
[11] STAR Collaboration: B I Abelev *et al*, *Phys. Rev.* **C79**, 034909 (2009)
[12] E Schnedermann, J Sollfrank and U Heinz, *Phys. Rev.* **C48**, 2462 (1993)
[13] D Teaney, J Lauret and E V Shuryak, *Phys. Rev. Lett.* **86**, 4783 (2001)
[14] D Teaney, J Lauret and E V Shuryak, arXiv:nucl-th/0110037
[15] P Huovinen, P F Kolb, U Heinz, P V Ruuskanen and S A Voloshin, *Phys. Lett.* **B503**, 58 (2001)
[16] P F Kolb, U Heinz, P Huovinen, K J Eskola and K Tuominen, *Nucl. Phys.* **A696**, 197 (2001)
[17] U Heinz and P Kolb, *Nucl. Phys.* **A702**, 269 (2002)
[18] F Retière and M A Lisa, *Phys. Rev.* **C70**, 044907 (2004)
[19] F-H Liu, *Phys. Rev.* **D62**, 074002 (2000)
[20] F-H Liu, *Nucl. Phys.* **A808**, 160 (2008)
[21] F-H Liu, *Nucl. Phys.* **A810**, 159 (2008)
F-H Liu, Q-W Lü, B-C Li and R Bekmirzaev, *Chin. J. Phys.* **49**, 601 (2011)
[22] F-H Liu and J-S Li, *Phys. Rev.* **C78**, 044602 (2008)
[23] E K G Sarkisyan and A S Sakharov, CERN-PH-TH/2004-213, arXiv:hep-ph/0410324
[24] E K G Sarkisyan and A S Sakharov, *AIP Conf. Proc.* **828**, 35 (2006)
[25] E Kokoulina, *Acta Phys. Pol.* **B35**, 295 (2004)
[26] E S Kokoulina and V A Nikitin, arXiv:hep-ph/0502224
[27] P F Ermolov, E S Kokoulina, E A Kuraev, A V Kutov, V A Nikitin, A A Pankov, I A Roufanov and N K Zhidkov, arXiv:hep-ph/0503254
[28] BRAHMS Collaboration: H-Y Yang, *J. Phys.* **G34**, S619 (2007)
[29] PHENIX Collaboration: A Adare *et al*, *Phys. Rev. Lett.* **101**, 162301 (2008)
[30] PHENIX Collaboration: A Adare *et al*, *Phys. Rev. Lett.* **98**, 232002 (2007)
[31] PHENIX Collaboration: A Bickley, *J. Phys.* **G34**, S779 (2007)
[32] NA50 Collaboration: B Alessandro *et al*, *Eur. Phys. J.* **C48**, 329 (2006)
[33] PHENIX Collaboration: A Adare *et al*, *Phys. Rev.* **C77**, 024912 (2008)
[34] PHENIX Collaboration: J T Mitchell, arXiv:nucl-ex/0701079
[35] PHENIX Collaboration: A Adare *et al*, *Phys. Rev. Lett.* **101**, 232301 (2008)
[36] PHENIX Collaboration: A Adare *et al*, *Phys. Rev.* **D83**, 052004 (2011)
[37] CMS Collaboration: S Chatrchyan *et al*, *J. High Energy Phys.* **08**, 086 (2011)
[38] G Wilk and Z Włodarczyk, *Eur. Phys. J.* **A40**, 299 (2009)